Journal of Colloid and Interface Science 530 (2018) 675–685

Contents lists available at ScienceDirect

Journal of Colloid and Interface Science

journal homepage: www.elsevier.com/locate/jcis

Regular Article

Periodic energy conversion in an electric-double-layer capacitor

Imri Atlas, Guy Z. Ramon *

The Nancy and Stephen Grand Technion Energy Program, and Department of Civil & Environmental Engineering, Technion - Israel Institute of Technology, Haifa 32000, Israel

GRAPHICAL ABSTRACT

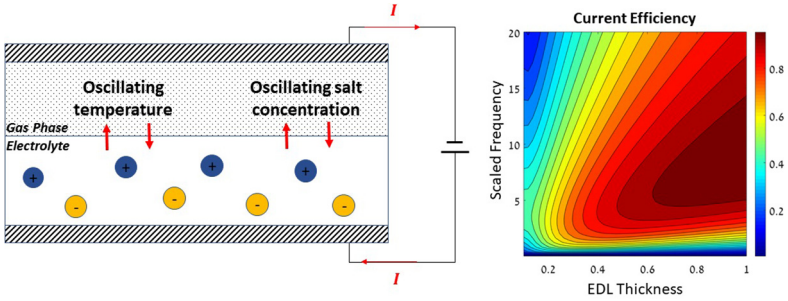

ARTICLE INFO

Article history:
Received 27 April 2018
Revised 13 June 2018
Accepted 15 June 2018
Available online 20 June 2018

Keywords:
Electric double layer capacitor
Energy harvester
Oscillatory excitation
Poisson-Nernst-Planck equations

ABSTRACT

Electrostatic conversion devices operate through periodic modulation of capacitance. Such devices have a wide range of configurations, involving either changes in permittivity, electrode-plate spacing or wetting area. The presented study examines, theoretically, a potential configuration of an electric-double-layer capacitor (EDLC)-based transducer, as it converts concentration and temperature oscillations into an electric alternating current. A constant voltage applied at the EDLC electrodes results in the formation of two opposite-sign EDLs, and an electric current is generated when ionic charges pass from one EDL to the other. In the examined configuration, this ionic charge transfer is induced by boundary modulation of temperature and/or concentration. To capture the oscillating dynamics of the ion distribution and ion flux, we solve the full set of Poisson-Nernst-Planck (PNP) equations coupled with the energy equation. We find that the transducer's optimal conditions for conversion, for which the device's frequency response is maximized, are governed by three main factors: low irreversible Joule heating, confined geometry, where the capacitor thickness is a close as possible to the EDL's characteristic screening length, and, most importantly, 'tuning' the system to a resonance frequency dictated by the interplay between geometry and characteristic time scales for mass and heat diffusion.

1. Introduction

Capacitive or electrostatic energy conversion devices harness mechanical vibrational energy to produce electricity through a variable capacitor. These devices typically serve as energy harvesters, scavenging energy from small amplitude ambient vibrations, intended for self-powered electronic systems and remote sensors [1–4]. An electrostatic parallel-plate capacitor stores electric energy by separating opposite charges with a dielectric inserted between the two conductive plates. When maintaining constant voltage V between the plates, the charge stored in a capacitor equals $Q = CV$, where C is the capacitance. In equilibrium, the parallel plate capacitance equals $C = A\varepsilon/d$, where A is the plate area, ε is the permittivity of the dielectric material and d is the plate separation. Vibrations may induce capacitance

* Corresponding author.
E-mail address: ramong@technion.ac.il (G.Z. Ramon).

https://doi.org/10.1016/j.jcis.2018.06.034
0021-9797/

variations by changes to one or more of the following: (1) overlapping area, (2) permittivity, and (3) gap spacing [5].

Electric double layer capacitors (EDLC), also known as electrochemical capacitors or super capacitors, are a class of capacitors that store electric energy at the interface between an electrolyte and a solid electrode [6]. In this case, the charge is separated by two neighboring phases or layers in an interfacial structure known as the electric double layer [7]. According to the Gouy-Chapman model [8], the capacitance of the EDLC with a fully dissociated, symmetric 1:1 salt at low applied voltages ($VF/RT \ll 1$) is $C = A\varepsilon/\lambda_D$, analogous to the capacitance of a parallel-plate capacitor. Here, A is the electrode's surface area, T is the temperature, F is Faraday's constant, R is the universal gas constant and the effective 'plate separation' is represented by the Debye length $\lambda_D = \sqrt{\varepsilon RT/2F^2 c_\infty}$, where ε is the solvent permittivity and c_∞ is the solution's bulk concentration. The Debye length is the characteristic distance from the electrode, over which excess ionic charges decay, eventually reaching the electro-neutral bulk solution.

Unlike conventional EDLCs, capacitive energy harvesting devices and transducers do not store energy but, rather, convert mechanical work, heat or salinity gradients into electrical energy by modulating the EDLC capacitance [9]. The analogy between the systems suggests that EDLC capacitance variations could be achieved in a similar fashion to that employed for parallel plate-based harvesters. Overlapping-area capacitance changes have been demonstrated through mechanical modulation of the EDL at the interfacial areas of a liquid bridge between two conducting plates [10–12]. Permittivity capacitance change can be achieved, for instance, by displacement of a moveable liquid dielectric or electrolyte droplet. This technique takes advantage of the significant difference in permittivity between the liquid and air [13,14]. EDLC 'plate spacing' capacitance change is achieved by alternating the Debye length λ_D. This deformation can be induced by mechanical fluctuations [15,16] or by 'Capacitive Double Layer Expansion' which was originally implemented by Brogioli [17]. The latter technique utilizes the Debye length's dependence on salt concentration. This technique's working principle inspired the development of several technologies, each one harvesting energy from a different source: (1) Energy extraction from salinity gradients between sea water and fresh water streams, known as 'Capacitive Mixing' (CapMix) [18,19]. Capacitive mixing can also serve as means of extracting energy from mixing sea water and acidic wastewater [20]. (2) Energy extraction from the concentration difference between CO_2, from power plant exhaust gas, and ambient air [21,22]. (3) Energy extraction from temperature gradients between two heat reservoirs [23] - this technique exploits the Debye length's dependence on the solution's temperature rather than its bulk concentration. All mentioned CDLE technologies harvest energy utilizing the the same charge-constrained electrostatic cycle [3] where the capacitance is lowered (by Debye length increase) at a constant charge.

Inspired by the concept of electric current generation in an EDLC through concentration/temperature modulation, we conceptualize a periodic, EDLC-based energy transducer. A constant applied voltage at the electrodes forms two EDLs of opposite signs in the vicinity of each electrode, and an electric current is generated when ionic charges pass from one EDL to the other. This initial ionic charge transfer is attained by periodically altering the balance between the electro-migration and mass diffusion of the ions. This alteration is driven by boundary modulation of either an electrically-neutral ion flux (forcing a concentration gradient) or heat flux (forcing an ion-mobility gradient). When the capacitance oscillations of an EDL are lower than the nominal value dictated by the equilibrium state, ionic charges are released. In the presented study, we are motivated by the challenge of designing a reliable transducer capable of converting temperature and composition oscillations into an electric current, with no moving parts. One may envision the integration of such a transducer with other technologies where temperature and pressure oscillations are induced, such as thermoacoustic engines [24] and oscillating heat pipes [25], providing a reliable means of energy conversion.

In what follows, we present the formulation of a mathematical model describing the physical response and performance of a transducer of this kind. This model can help identify the critical range of parameters in which the performance and efficiency are optimal, attaining the maximum current density amplitude. The ion concentration, electric potential and temperature fields (and the generated electric current) are found through the solution of the Poisson-Nernst-Planck (PNP) equations, coupled with the energy equation. Three possible configurations are examined in terms of the periodic input, namely salt, temperature or a combination of both.

2. Model formulation

The conceptualized system considers two basic configurations, based on a typical electrochemical cell, consisting of two charged electrodes separated by an electrolyte. The voltage between the two electrodes, V, is kept constant by an external power source. The boundary at $x = 0$ is assumed to be a non-penetrable and thermally insulated electrode. The electrolyte's boundary at $x = L$ defines the transducer type. For a temperature-driven transducer, the boundary at $x = L$ is an impenetrable electrode with an imposed oscillating temperature (see schematic drawing in Fig. 1a), while for a concentration-driven transducer a possible configuration can be that of two electrodes separated by two layers - an electrolyte film and a dielectric gas phase - this enables a soluble gas to enter and exit the electrolyte layer, as in an absorption system. In this case, the boundary at $x = L$ is the interface between the electrolyte and gas. Pressure or temperature oscillations in the

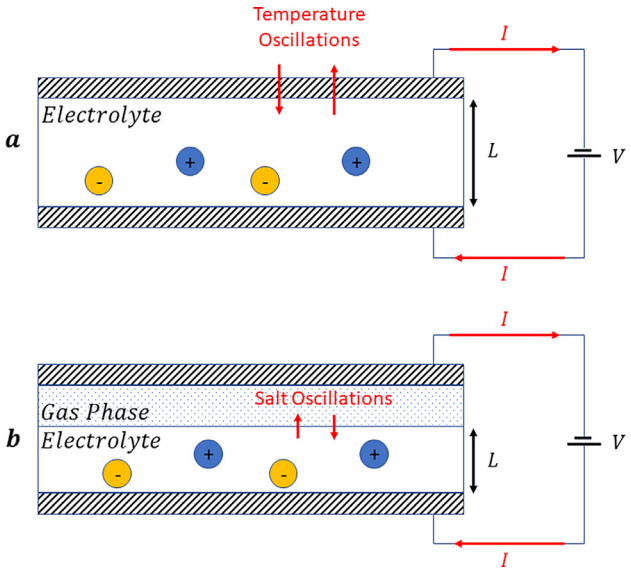

Fig. 1. A schematic representation of the EDL-based, capacitive transducer. **a.** Temperature-driven transducer, consisting of a typical electrochemical cell with a periodic variation of temperature on one side. **b.** Concentration-driven transducer, conceptualized as an electrolyte film in contact with a gas phase, in which temperature and composition changes are induced by pressure oscillations - a soluble gas component may thus sorb and de-sorb out of the electrolyte. The two layers are confined within a parallel-plate electrochemical cell.

gas phase, e.g. produced by a thermoacoustic engine [26], induce an oscillating concentration (and temperature) on the electrolyte's boundary. Assuming that the capacitance of the gas phase layer is much lower than the electrolyte's, due to material properties (the permittivity of the gas is much lower than the liquid), one may show that the linear electrostatic potential gradient across the dielectric gas phase is small (See schematic drawing in Fig. 1b). To keep a reasonable level of simplicity at this point, the gas phase dynamics are neglected within the presented framework.

2.1. Governing equations

In order to find the concentration ($c_{\pm}$, for the positive and negative ions, respectively), temperature (T) and electric potential (ϕ) distributions along the direction perpendicular to the electrodes, we solve the Poisson-Nernst-Planck (PNP) equations, coupled with the energy equation. For simplicity, we consider a fully dissociated symmetric 1:1 salt with equal, constant diffusivities. The dependence of the diffusivity on the electrolyte concentration is not accounted for, nor are the possible effects of the finite size of ions in the solution and at the electrode - as this model represents an initial step towards understanding the dynamics of such systems, we leave these aspects for future refinement and extensions.

We begin by casting the PNP equations into dimensionless form. The electrolyte layer thickness, L, is used as the reference length scale, and the "RC time" [27] - the EDL charging time $\tau_{RC} = \lambda_D L/D$ - as the characteristic time scale. The characteristic size of the EDL is given, naturally, by the Debye length $\lambda_D = \sqrt{\varepsilon RT/2F^2 c_n}$, where c_n is the the nominal salt concentration of the electrolyte prior to its polarization. The thermal voltage $\Phi = RT_0/F$ is used as a reference scale for the electrostatic potential and the temperature is scaled using the mean part of the applied temperature, T_0. Further, we define the mobility according to the Einstein relation: $v = \frac{D}{RT}$. Hence, the following dimensionless variables may be defined:

$$\widehat{x} = \frac{x}{L}, \qquad \widehat{t} = \frac{D}{\lambda_D L}t, \qquad \widehat{\phi} = \frac{F}{RT}\phi, \qquad \widehat{T} = \frac{T}{T_0}. \tag{1}$$

In addition, the dimensionless average salt concentration $\widehat{c}$ and average charge density $\widehat{\rho}$ are given by

$$\widehat{c} = \frac{c_+ + c_-}{2c_n}, \qquad \widehat{\rho} = \frac{c_+ - c_-}{2c_n}. \tag{2}$$

This formulation allows to conveniently distinguish between ionic charge transport and neutral salt transport [27–30].

The ion distribution satisfies the conservation of species given by the Nernst-Planck equations, which, in dimensionless form, read

$$\frac{\partial \widehat{c}}{\partial \widehat{t}} = \epsilon \frac{\partial^2 \widehat{c}}{\partial \widehat{x}^2} + \epsilon \frac{\partial}{\partial \widehat{x}}\left(\frac{\widehat{\rho}}{\widehat{T}}\frac{\partial \widehat{\phi}}{\partial \widehat{x}}\right), \tag{3}$$

$$\frac{\partial \widehat{\rho}}{\partial \widehat{t}} = \epsilon \frac{\partial^2 \widehat{\rho}}{\partial \widehat{x}^2} + \epsilon \frac{\partial}{\partial \widehat{x}}\left(\frac{\widehat{c}}{\widehat{T}}\frac{\partial \widehat{\phi}}{\partial \widehat{x}}\right). \tag{4}$$

The ionic charge density, $\widehat{\rho}$, is linked to the spatial variation of the potential through Poisson's equation of electrostatics, here given in dimensionless form as

$$-\epsilon^2 \frac{\partial^2 \widehat{\phi}}{\partial \widehat{x}^2} = \widehat{\rho}. \tag{5}$$

Finally, the temperature field is obtained through the dimensionless energy equation [31–33]

$$\frac{\partial \widehat{T}}{\partial \widehat{t}} = \epsilon Le \frac{\partial^2 \widehat{T}}{\partial \widehat{x}^2} + \epsilon \Pi \left[\frac{\partial \widehat{\rho}}{\partial \widehat{x}}\frac{\partial \widehat{\phi}}{\partial \widehat{x}} + \frac{\widehat{c}}{\widehat{T}}\left(\frac{\partial \widehat{\phi}}{\partial \widehat{x}}\right)^2\right]. \tag{6}$$

The second and third terms on the right-hand side represent the generalized Joule heating defined as the dot product of ionic current and negative of potential gradient [34–36]. This heating term is composed of, respectively, the electrostatic work due to to diffusion of ions within an electric field and the irreversible heat generation rate. Three important non-dimensional parameters appear in Eqs. (3)–(6):

$$\epsilon \equiv \lambda_D/L, \qquad Le \equiv \alpha/D, \qquad \Pi \equiv 2c_n R/\rho C_p, \tag{7}$$

where ϵ is the ratio of the Debye length to the electrolyte layer thickness, reflecting the EDL's relative thickness; Le is the ratio of thermal to mass diffusivity (known as the Lewis number); finally, Π (in which ρ is the mass density and C_p is the heat capacity) may be viewed as representative of the solution's characteristic osmotic pressure relative to its internal energy or, in other words, the resistance to concentration changes vs. the resistance to temperature changes. As already mentioned, material properties contained within the non-dimensional parameters are assumed constant and independent of temperature and composition [31–33].

2.2. Boundary conditions

For all cases considered, the following boundary conditions are imposed. At the lower electrode surface, $\widehat{x} = 0$, a constant potential is set (Eq. (8a)). The electrode is also considered impermeable (Eq. (8b) and (8c)) and insulated (Eq. (8d)),

$$\widehat{\phi} = \zeta, \tag{8a}$$

$$-\frac{\partial \widehat{c}}{\partial \widehat{x}} - \widehat{\rho}\frac{\partial \widehat{\phi}}{\partial \widehat{x}} = 0, \tag{8b}$$

$$-\frac{\partial \widehat{\rho}}{\partial \widehat{x}} - \widehat{c}\frac{\partial \widehat{\phi}}{\partial \widehat{x}} = 0, \tag{8c}$$

$$-\frac{\partial \widehat{T}}{\partial \widehat{x}} = 0, \tag{8d}$$

where $\zeta \equiv FV/RT$ is the scaled potential, representing the ratio of the applied voltage to the 'thermal voltage'. In addition, boundary conditions at $\widehat{x} = 1$ are (ground) potential (Eq. (9a)) and a vanishing electric current (Eq. (9b)). The latter condition maintains the overall solution electro-neutrality, as no ionic charge enters the system.

$$\widehat{\phi} = 0, \tag{9a}$$

$$\frac{\partial \widehat{\rho}}{\partial \widehat{x}} + \widehat{c}\frac{\partial \widehat{\phi}}{\partial \widehat{x}} = 0. \tag{9b}$$

We now turn to the oscillatory forcing imposed as a boundary condition at $\widehat{x} = 1$, according to each transducer configuration. For a concentration-driven transducer (Fig. 1.b), we have

$$\widehat{c} = \widehat{c_0} + \delta_s e^{i\widehat{\omega}\widehat{t}}, \tag{10a}$$

$$\widehat{T} = 1, \tag{10b}$$

where $\widehat{c_0}$ is the mean salt concentration at the the interface, δ_S is the oscillating salt concentration amplitude and $\widehat{\omega} \equiv \omega \lambda_D L/D$ is the ratio of the oscillation frequency to the 'RC frequency'. For a temperature-driven transducer (Fig. 1.a), we impose

$$\frac{\partial \widehat{c}}{\partial \widehat{x}} + \widehat{\rho}\frac{\partial \widehat{\phi}}{\partial \widehat{x}} = 0, \tag{11a}$$

$$\widehat{T} = 1 + \delta_T e^{i\widehat{\omega}\widehat{t}}, \tag{11b}$$

where δ_T is the oscillating temperature amplitude.

Finally, the boundary conditions for the combined case (Fig. 1. b), are

$$\widehat{c} = \widehat{c}_0 + \delta_T A e^{i\widehat{\omega t}}, \tag{12a}$$

$$\widehat{T} = 1 + \delta_T e^{i\widehat{\omega t}}. \tag{12b}$$

where $A \equiv \delta_s/\delta_T \angle\theta$ is the ratio of the oscillating amplitudes of concentration to temperature, with θ representing the phase angle between the oscillating temperature and concentration.

2.3. Solution for small amplitudes

For small amplitudes, $\delta \ll 1$ (either δ_s or δ_T) we expand all variables as the sum of a mean part of $O(1)$ (subscript m) and complex, oscillatory, time-dependent perturbation (subscript p) of $O(\delta)$, i.e. $g(x,t) = g_m(x) + g_p(x)e^{i\widehat{\omega t}}$ where g represents $\widehat{c}$, $\widehat{\rho}$, $\widehat{\phi}$ and $\widehat{T}$ [37]. Additionally, we limit $\widehat{c}_p \leqslant \widehat{c}_m$ and $\widehat{T}_p \leqslant \widehat{T}_m$ to maintain a physical solution (no negative concentration or temperature allowed). Next, we substitute the variable expansions into Eqs. (3)–(6) and boundary conditions (8a)–(12b) and obtain a problem at each order. First, we solve the mean problem at $O(1)$, characterized by stationary boundary conditions. Using solutions to the mean problems we solve the oscillating fields, at $O(\delta)$. In what follows, we present the system of equations and their boundary conditions. Equations Eqs. (13)–(23) were solved using MATLAB's bvp4c solver.

At leading order, $O(1)$, we have

$$\frac{\partial \widehat{c}_m}{\partial \widehat{x}} + \frac{\widehat{\rho}_m}{\widehat{T}_m}\frac{\partial \widehat{\phi}_m}{\partial \widehat{x}} = 0, \tag{13}$$

$$\frac{\partial \widehat{\rho}_m}{\partial \widehat{x}} + \frac{\widehat{c}_m}{\widehat{T}_m}\frac{\partial \widehat{\phi}_m}{\partial \widehat{x}} = 0, \tag{14}$$

$$\frac{\partial^2 \widehat{\phi}_m}{\partial \widehat{x}^2} = -\frac{1}{\epsilon^2}\widehat{\rho}_m. \tag{15}$$

The zero charge flux degenerates the energy equation, at leading order, into a steady-state conduction equation, de-coupling it from the PNP equations,

$$\frac{\partial^2 \widehat{T}_m}{\partial \widehat{x}^2} = 0, \tag{16}$$

with the boundary conditions, at $\widehat{x} = 0$,

$$\widehat{\phi}_m = \zeta, \tag{17a}$$

$$\frac{\partial \widehat{c}_m}{\partial \widehat{x}} + \frac{\widehat{\rho}_m}{\widehat{T}_m}\frac{\partial \widehat{\phi}_m}{\partial \widehat{x}} = 0, \tag{17b}$$

$$\frac{\partial \widehat{\rho}_m}{\partial \widehat{x}} + \frac{\widehat{c}_m}{\widehat{T}_m}\frac{\partial \widehat{\phi}_m}{\partial \widehat{x}} = 0, \tag{17c}$$

$$\frac{\partial \widehat{T}_m}{\partial \widehat{x}} = 0, \tag{17d}$$

and, at $\widehat{x} = 1$,

$$\widehat{\phi}_m = 0, \tag{18a}$$

$$\widehat{c}_m = \widehat{c}_0, \tag{18b}$$

$$\widehat{\rho}_m = \widehat{\rho}_0, \tag{18c}$$

$$\widehat{T}_m = 1, \tag{18d}$$

where $\widehat{\rho_0}$ is the mean charge density.

The mean, time-averaged problem is characterized by a constant salt concentration and charge density flux. With the boundary conditions of an impermeable electrode at $\widehat{x} = 0$ (Eqs. (17b) and (17c)) we may determine that these fluxes are equal to zero at any point. Integrating Eq. (16) further reveals that the mean heat flux across the solution is also constant and equal to zero due to the insulated electrode at $\widehat{x} = 0$ (B.C. (17d)). Hence, the temperature profile, at leading order, is uniform, i.e. $\widehat{T}_m = 1$. In order to solve for the concentration and charge density distributions we must modify the boundary conditions at $\widehat{x} = 1$ since, in the case of the concentration-driven transducer, the value of $\widehat{c}_0$ at the boundary (Eq. (17d)) is unknown a priori, as only the amplitude of the oscillating concentration at the boundary is prescribed. Furthermore, in the case of the oscillating temperature transducer, the additional zero flux condition at $\widehat{x} = 1$ is redundant since we have already determined that the mean flux equals zero. Nevertheless, the notion that the mean problem is time-independant allows us to determine that the mean concentration in the solution is equal to its nominal value multiplied by the capacitor thickness and that the mean charge has to be zero since the solution is, overall, electro-neutral. In this manner, in order to make the mean problem solvable, we convert these two zero flux boundary conditions at the boundary $\widehat{x} = 1$ into two integral constraints [38],

$$\int_0^1 \widehat{c}_m d\widehat{x} = 1, \tag{19a}$$

$$\int_0^1 \widehat{\rho}_m d\widehat{x} = 0, \tag{19b}$$

which signify the conservation of the overall electrolyte mass and electro-neutrality, respectively.

Next, we turn to the oscillating, $O(\delta)$ problem, for which we write the PNP equations

$$\frac{i\widehat{\omega}}{\epsilon}\widehat{c}_p = \frac{\partial^2 \widehat{c}_p}{\partial \widehat{x}^2} + 2\frac{\widehat{T}_p}{\widehat{T}_m}\frac{\partial^2 \widehat{c}_m}{\partial \widehat{x}^2} + \frac{1}{\widehat{T}_m}\frac{\partial}{\partial \widehat{x}}\left(\widehat{\rho}_p\frac{\partial \widehat{\phi}_m}{\partial \widehat{x}} + \widehat{\rho}_m\frac{\partial \widehat{\phi}_p}{\partial \widehat{x}}\right) + \frac{\widehat{T}_p}{\widehat{T}_m}\frac{\partial}{\partial \widehat{x}}\left(\widehat{\rho}_m\frac{\partial \widehat{\phi}_m}{\partial \widehat{x}}\right) - \frac{1}{\widehat{T}_m^2}\left(\widehat{\rho}_m\frac{\partial \widehat{\phi}_m}{\partial \widehat{x}}\frac{\partial \widehat{T}_p}{\partial \widehat{x}} - \widehat{\rho}_m\frac{\partial \widehat{\phi}_p}{\partial \widehat{x}}\frac{\partial \widehat{T}_m}{\partial \widehat{x}} - \widehat{\rho}_p\frac{\partial \widehat{\phi}_m}{\partial \widehat{x}}\frac{\partial \widehat{T}_m}{\partial \widehat{x}}\right), \tag{20}$$

$$\frac{i\widehat{\omega}}{\epsilon}\widehat{\rho}_p = \frac{\partial^2 \widehat{\rho}_p}{\partial \widehat{x}^2} + 2\frac{\widehat{T}_p}{\widehat{T}_m}\frac{\partial^2 \widehat{\rho}_m}{\partial \widehat{x}^2} + \frac{1}{\widehat{T}_m}\frac{\partial}{\partial \widehat{x}}\left(\widehat{c}_p\frac{\partial \widehat{\phi}_m}{\partial \widehat{x}} + \widehat{c}_m\frac{\partial \widehat{\phi}_p}{\partial \widehat{x}}\right) + \frac{\widehat{T}_p}{\widehat{T}_m}\frac{\partial}{\partial \widehat{x}}\left(\widehat{c}_m\frac{\partial \widehat{\phi}_m}{\partial \widehat{x}}\right) - \frac{1}{\widehat{T}_m^2}\left(\widehat{c}_m\frac{\partial \widehat{\phi}_m}{\partial \widehat{x}}\frac{\partial \widehat{T}_p}{\partial \widehat{x}} - \widehat{c}_m\frac{\partial \widehat{\phi}_p}{\partial \widehat{x}}\frac{\partial \widehat{T}_m}{\partial \widehat{x}} - \widehat{c}_p\frac{\partial \widehat{\phi}_m}{\partial \widehat{x}}\frac{\partial \widehat{T}_m}{\partial \widehat{x}}\right), \tag{21}$$

$$\frac{\partial^2 \widehat{\phi}_p}{\partial \widehat{x}^2} = -\frac{1}{\epsilon^2}\widehat{\rho}_p, \tag{22}$$

and the energy equation,

$$\frac{i\widehat{\omega}}{\epsilon Le}\widehat{T}_p = \frac{\partial^2 \widehat{T}_p}{\partial \widehat{x}^2} + \frac{\widehat{T}_p}{\widehat{T}_m}\frac{\partial^2 \widehat{T}_m}{\partial \widehat{x}^2} + \frac{\pi}{Le}\left[\frac{\partial \widehat{\rho}_m}{\partial \widehat{x}}\frac{\partial \widehat{\phi}_p}{\partial \widehat{x}} + \frac{\partial \widehat{\rho}_p}{\partial \widehat{x}}\frac{\partial \widehat{\phi}_m}{\partial \widehat{x}} + \frac{\widehat{T}_p}{\widehat{T}_m}\frac{\partial \widehat{\rho}_m}{\partial \widehat{x}}\frac{\partial \widehat{\phi}_m}{\partial \widehat{x}} + \frac{\widehat{c}_p}{\widehat{T}_m}\left(\frac{\partial \widehat{\phi}_m}{\partial \widehat{x}}\right)^2\right]. \tag{23}$$

The oscillating forcing appears through the boundary conditions. For the concentration-driven case, we have

$$\widehat{c}_p = 1, \tag{24a}$$

$$\widehat{T}_p = 0, \tag{24b}$$

and for the temperature-driven case,

$$\widehat{T}_m\frac{\partial \widehat{c}_p}{\partial \widehat{x}} + \widehat{T}_p\frac{\partial \widehat{c}_m}{\partial \widehat{x}} + \widehat{\rho}_m\frac{\partial \widehat{\phi}_p}{\partial \widehat{x}} + \widehat{\rho}_p\frac{\partial \widehat{\phi}_m}{\partial \widehat{x}} = 0, \tag{25a}$$

$$\widehat{T}_p = 1. \tag{25b}$$

Finally, the combination of concentration and temperature oscillations,

$$\widehat{c}_p = A, \tag{26a}$$

$$\widehat{T}_p = 1. \tag{26b}$$

The remaining boundary conditions at $\widehat{x} = 0$ become

$$\widehat{\phi}_p = 0, \tag{27a}$$

$$\widehat{T}_m \frac{\partial \widehat{c}_p}{\partial \widehat{x}} + \widehat{T}_p \frac{\partial \widehat{c}_m}{\partial \widehat{x}} + \widehat{\rho}_m \frac{\partial \widehat{\phi}_p}{\partial \widehat{x}} + \widehat{\rho}_p \frac{\partial \widehat{\phi}_m}{\partial \widehat{x}} = 0, \tag{27b}$$

$$\widehat{T}_m \frac{\partial \widehat{\rho}_p}{\partial \widehat{x}} + \widehat{T}_p \frac{\partial \widehat{\rho}_m}{\partial \widehat{x}} + \widehat{c}_m \frac{\partial \widehat{\phi}_p}{\partial \widehat{x}} + \widehat{c}_p \frac{\partial \widehat{\phi}_m}{\partial \widehat{x}} = 0, \tag{27c}$$

$$\frac{\partial \widehat{T}_p}{\partial \widehat{x}} = 0. \tag{27d}$$

And the remaining conditions at $\widehat{x} = 1$,

$$\widehat{\phi}_p = 0, \tag{28a}$$

$$\widehat{T}_m \frac{\partial \widehat{\rho}_p}{\partial \widehat{x}} + \widehat{T}_p \frac{\partial \widehat{\rho}_m}{\partial \widehat{x}} + \widehat{c}_m \frac{\partial \widehat{\phi}_p}{\partial \widehat{x}} + \widehat{c}_p \frac{\partial \widehat{\phi}_m}{\partial \widehat{x}} = 0. \tag{28b}$$

2.4. Calculation of the current density

Once the distributions of $\widehat{c}$, $\widehat{\rho}$, $\widehat{\phi}$ and $\widehat{T}$ are found, we can calculate the electric current, $\widehat{I}$, generated by the transducer. The ionic charge flux at any point in the solution is

$$\widehat{J}\left(\widehat{x},\widehat{t}\right) = Re\left\{\left(\frac{\partial \widehat{\rho}_p}{\partial \widehat{x}} + \frac{\widehat{T}_p}{\widehat{T}_m}\frac{\partial \widehat{\rho}_m}{\partial \widehat{x}} + \frac{\widehat{c}_m}{\widehat{T}_m}\frac{\partial \widehat{\phi}_p}{\partial \widehat{x}} + \frac{\widehat{c}_p}{\widehat{T}_m}\frac{\partial \widehat{\phi}_m}{\partial \widehat{x}}\right)e^{i\widehat{\omega}\widehat{t}}\right\}, \tag{29}$$

in which $Re[\cdot]$ is the real part of a complex quantity. For convenience in subsequent calculations, the transition point between the two EDLs, where the charge density equals zero, is defined as $\widehat{x}_0$. The location of this point shifts in time as one EDL expands and the other contracts. The ionic charge flux through this point is equal to the generated electric current $\widehat{I} = \widehat{J}(\widehat{x}_0, t)$. To obtain the dimensional current density, multiply by $2FDc_n/\lambda_D$.

3. Results and discussion

Through the solution to our model equations, we wish to identify the parameter regime for which the transducer's response to the oscillations is optimal, in terms of the current amplitude. To this end, we define the 'efficiency',

$$\eta \equiv \frac{\widehat{I}_{amp}(\epsilon,\ \mathrm{Le},\ \widehat{\omega},\ \theta,\ \Pi)}{\widehat{I}_{amp}^{max}},$$

as the ratio of the generated to the maximal scaled current amplitude, achievable for a given set of parameters. Note that this scaling is used for convenience, with the goal of identifying the conditions leading to the best response of the transducer, and not necessarily the greatest power output. In the same spirit, we note that the choice of parameters is made in order to facilitate a clear and intuitive distinction between different regimes rather than a strictly physical realization of a device.

3.1. The time-averaged problem: Thin versus thick EDLs

Before examining the EDLC's frequency response and current generation we begin with the solution to the mean problem, at $O(1)$, which describes a constant applied voltage at the electrodes and the resulting polarization of the electrolyte. In this case, two EDLs of opposite signs are formed in the vicinity of each electrode (Fig. 2). In the limit of thin EDLs, i.e., $\epsilon \equiv \frac{\lambda_D}{L} \ll 1$, they appear as boundary layers close to the electrodes. Within these boundary layers, $\widehat{c}$, $\widehat{\rho}$, and $\widehat{\phi}$ decay exponentially to a value dictated by bulk properties outside the boundary layers - the charge-neutral, well-mixed electrolyte solution. This 'bulk region' is characterized by a zero charge density as well as uniform average salt concentration and potential gradient (Fig. 2.a–c). In contrast, for thick EDLs, $\epsilon \sim 1$, where the Debye length is on the order of the capacitor thickness, the two EDLs occupy the entire domain, in which case, the charge density and potential profiles are linear and the 'bulk region' reduces to a single point, (Fig. 2.a–c).

3.2. The effect of characteristic time scales

The EDLC's frequency response can be understood in terms of characteristic time scales [27,39,40], namely $\tau_\omega = 1/\omega$, the oscillation period, and $\tau_{RC} = \lambda_D L/D$, the characteristic relaxation time of the electrochemical cell, representing the time scale of EDL charging (and eventually the generated current's response time). In addition, we may define τ_C, the characteristic time scale of the capacitance variation, which depends on the driving mechanism of the transducer - concentration, temperature or both. In the concentration-driven case, $\tau_C = \tau_D \equiv L^2/D$, where τ_D is the diffusive time scale. In the temperature-driven case, $\tau_C = \tau_\alpha \equiv L^2/\alpha$, where τ_α is the conductive time scale. The ordering $\tau_{RC} : \tau_C : \tau_\omega$ dictates the nature of the frequency response and, hence, the current efficiency. The ratio τ_C/τ_ω expresses the ability of the concentration or temperature fields to respond to the oscillatory forcing at the boundary. In the concentration-driven case, $\tau_C/\tau_\omega = \omega/\epsilon = \omega L^2/D$, while in the temperature-driven case, $\tau_C/\tau_\omega = \omega/\epsilon \mathrm{Le} = \omega L^2/\alpha$. Most importantly, the ratio τ_{RC}/τ_C represents the ability of the EDL to respond to the capacitance variations through diffusive charging

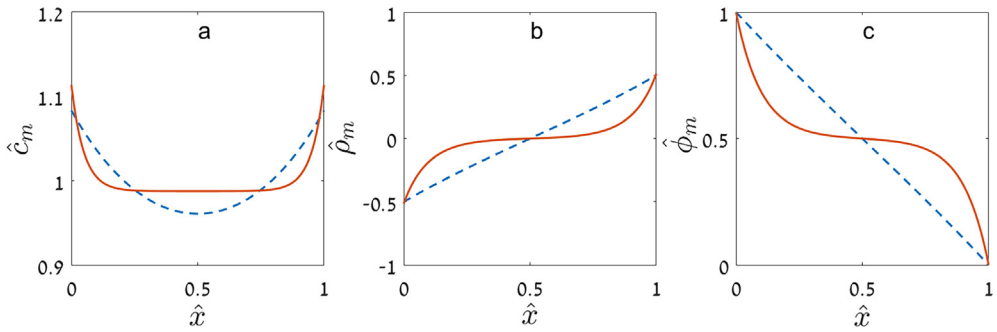

Fig. 2. Mean profiles of (a) dimensionless average salt concentration $\widehat{c}_m$ (b) dimensionless charge density $\widehat{\rho}_m$. (c) dimensionless potential $\widehat{\phi}_m$. Calculations made for a scaled applied voltage, $\zeta = 1$. Thin EDLs ($\epsilon = 0.1$) decay exponentially to a value dictated by bulk properties outside the boundary layers (solid red). For $\epsilon = 1$ the two EDLs occupy the entire domain and both the charge density and potential profiles are linear, while the 'bulk' region reduces to a single point (blue dash). (For interpretation of the references to colour in this figure legend, the reader is referred to the web version of this article.)

and discharging - when this ratio is small, the forcing is too fast for the capacitor to respond effectively, and conversely, when the forcing is slow, the system is expected to be quasi-steady where the entire domain has ample time to equilibrate while the temperature or concentration at the boundary oscillate. We therefore expect to see an optimum, 'tuned' frequency for a given system, a combination of the forcing frequency, the geometry and the transport coefficients.

3.3. Concentration and temperature-driven transducers

For simplicity, we present the frequency response in the limit of $\Pi \ll 1$, eliminating any generalized Joule heating. This assumption allows us to de-couple the energy Eq. (23) from the PNP Eqs. (20)–(22) and to solve the temperature profile analytically. The response efficiency, η, in the concentration-driven case, is shown in Fig. 3, for different values of ϵ. In this case the temperature profile is simply $\widehat{T} = 1$. The frequency response of the current efficiency in the temperature-driven case is shown in Fig. 4, for different values of *Le*. In this case the temperature profile is

$$\widehat{T} = 1 + \delta_T Re \left\{ \frac{\cosh\left(\sqrt{\frac{i\widehat{\omega}}{\epsilon Le}}\widehat{x}\right)}{\cosh\left(\sqrt{\frac{i\widehat{\omega}}{\epsilon Le}}\right)} e^{i\widehat{\omega}\widehat{t}} \right\}. \tag{30}$$

The most evident conclusion from Figs. 3 and 4 is that higher values of τ_{RC}/τ_C yield greater current efficiency.

3.3.1. The effect of ϵ and *Le*

In the concentration-driven case, where $\tau_{RC}/\tau_D = \epsilon$, a thicker EDL responds more efficiently. In the limit of thin EDLs, $\epsilon \ll 1$, the capacitance variation time scale is significantly higher than the relaxation time, meaning that the response efficiency is not limited by charge diffusion within the EDL, but rather by the diffusion of ions through the bulk region. In this case, the released ionic charge (due to EDL capacitance variations) must pass a 'bulk' region that separates the two EDLs. In this region, the charge flux is mostly dominated by electro-migration of ions (the contribution of diffusion is negligible due to the uniform concentration), making the electric current proportional to the potential gradient, i.e., $\widehat{J}_{\widehat{\rho}} \sim \frac{\partial \phi}{\partial \widehat{x}}$. The fact that the electric current is governed by Ohm's law suggests that this bulk region is 'resistive'. Minimizing this parasitic internal resistance and maximizing the electrolyte's capacitance by increasing the thickness of the EDLs results in greater transduction efficiency. In the temperature-driven case, $\tau_{RC}/\tau_\alpha = \epsilon Le$, a high thermal diffusivity may compensate the charge transfer for thin EDLs separated by a significant 'resistive' bulk region.

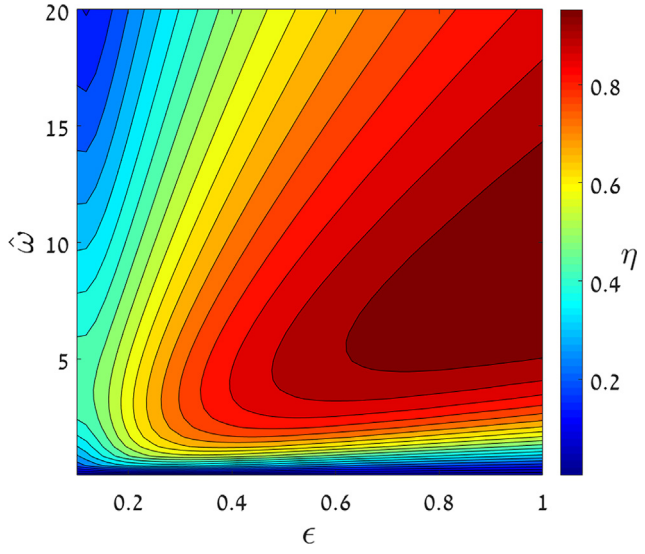

Fig. 3. Current efficiency η of the concentration-driven transducer versus ϵ and $\widehat{\omega}$. Calculations made for a scaled applied voltage $\zeta = 1$ and scaled boundary amplitude $\delta_s = 0.1$.

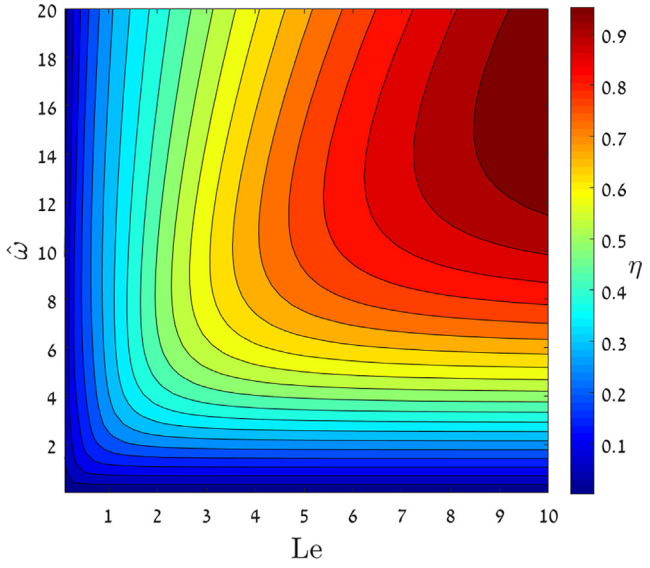

Fig. 4. Current efficiency η of the temperature-driven transducer versus *Le* and $\widehat{\omega}$. Calculations made for a scaled applied voltage $\zeta = 1$, thick EDL $\epsilon = 1$, and scaled boundary amplitude $\delta_T = 0.1$.

3.3.2. The effect of the oscillation frequency

Another conclusion from both Figs. 3 and 4 is that every given value of ϵ or *Le* is characterized by two main scaled frequency

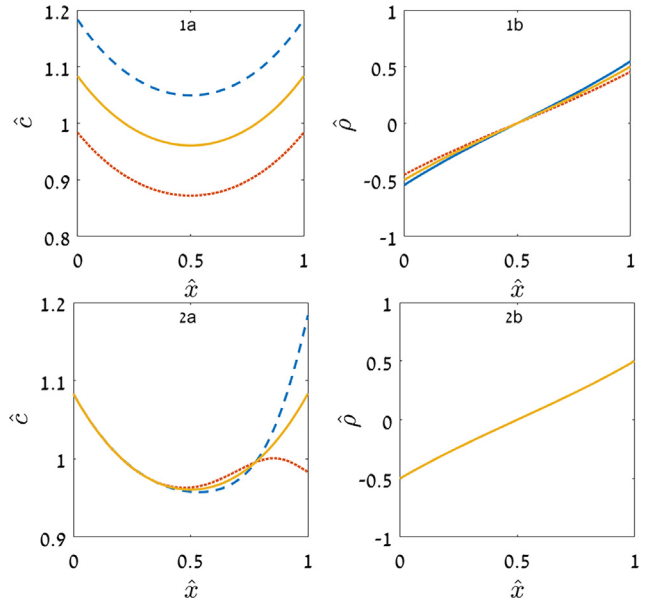

Fig. 5. Concentration-driven transducer profiles of: (a) dimensionless average salt concentration $\hat{c}$ (b) dimensionless charge density $\hat{\rho}$ for (1) low scaled frequency $\widehat{\omega} = 0.1$ and (2) high scaled frequency $\widehat{\omega} = 100$. $\widehat{\omega}\widehat{t} = 0$ (blue dash), $\widehat{\omega}\widehat{t} = \pi$ (red dot) and mean (yellow solid). Calculations made for a scaled applied voltage $\zeta = 1$, thick EDL $\epsilon = 1$ and scaled boundary amplitude $\delta_s = 0.1$. (For interpretation of the references to colour in this figure legend, the reader is referred to the web version of this article.)

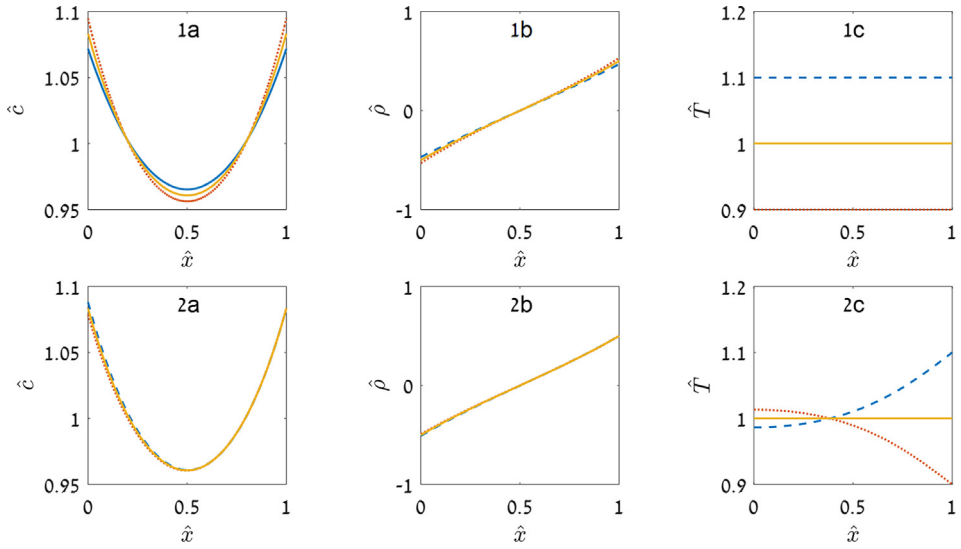

Fig. 6. Temperature-driven transducer profiles of: (a) dimensionless average salt concentration $\hat{c}$ (b) dimensionless charge density $\hat{\rho}$ (c) dimensionless temperature for (1) low scaled frequency $\widehat{\omega} = 0.1$ and (2) high scaled frequency $\widehat{\omega} = 100$. $\widehat{\omega}\widehat{t} = 0$ (blue dash), $\widehat{\omega}\widehat{t} = \pi$ (red dot) and mean (yellow solid). Calculations made for a scaled applied voltage $\zeta = 1$, thick EDL $\epsilon = 1$, $Le = 10$ and scaled boundary amplitude $\delta_T = 0.1$. (For interpretation of the references to colour in this figure legend, the reader is referred to the web version of this article.)

regimes $\widehat{\omega} \sim \tau_C/\tau_\omega$. For small $\widehat{\omega}$, the current amplitude increases with $\widehat{\omega}$, and the highest frequency in this regime may be considered as the 'resonant' frequency, beyond which a further increase reduces the response efficiency of the transduction. When $\tau_C/\tau_\omega \ll 1$, the forcing oscillation period is significantly larger than the capacitance relaxation time (τ_D or τ_α), allowing the concentration or temperature field to respond to the changes at the boundary. Furthermore, this regime is characterized by a uniform spatial response of the concentration or the temperature to the periodic excitation: in both cases (Fig. 61) there is no phase difference and equal amplitude between each cross-section and the boundary. In this regime, the oscillating EDL expansion mechanism is the most efficient when charge density accumulation close to one electrode is instantly compensated by depletion at the opposite side (Figs. 51b and 61b). As long as the condition $\tau_C/\tau_\omega < 1$ is maintained, an enhanced current amplitude may be achieved with increased scaled frequency.

Conversely, for $\tau_C/\tau_\omega \gg 1$, the oscillation period is significantly smaller than the capacitance relaxation time, and so the concentration or temperature fields do not have sufficient time to respond to the oscillation at the boundary. This regime is characterized by a non-uniform spatial response, where phase differences between each cross-section and the boundary emerge and grow as the scaled frequency increases. The amplitude of the concentration (Fig. 5.2) and temperature (Fig. 6.2) at each cross-section is lowered depending on its distance from the boundary. The transduction is least efficient once any further increase in the frequency results in lower charge density amplitude. Finally, at extremely high scaled frequencies, the profiles approach the mean profiles, as seen in Figs. 5.2b and 6.2b.

3.4. The effect of the phase difference in a combined temperature and concentration-driven mode

After investigating the frequency responses of both concentration and temperature-driven cases, we turn to examine the combined case, and the effect of phase differences between them, on current efficiency. To capture the sole effect of the phase difference we set $A = 1$ and $Le = 1$. In this case, where the non-dimensional boundary amplitudes are equal and also conductive and diffusive time scales are of the same order, we do not bias the electrochemical cell towards any EDL expansion mechanism. The frequency response of η in the combined case is shown in Fig. 7a, for different values of θ.

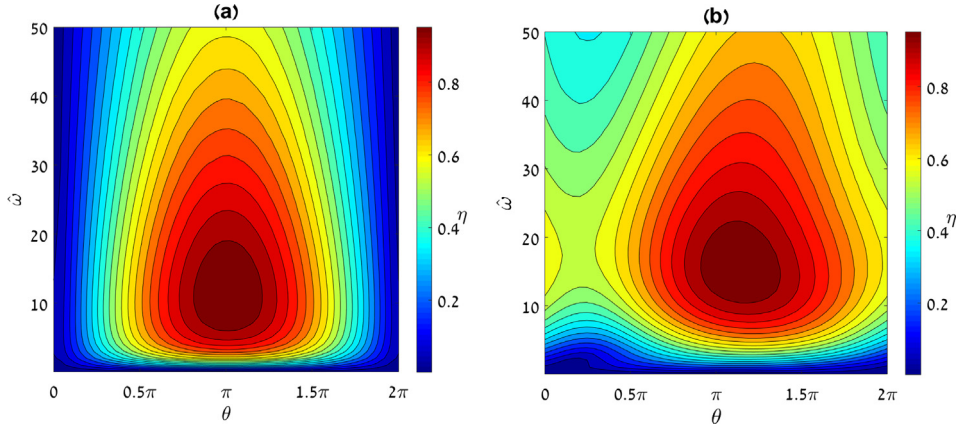

Fig. 7. Current efficiency η for the combined concentration- and temperature-driven transducer versus θ and $\widehat{\omega}$. Calculations made for a scaled applied voltage $\zeta = 1$ and scaled boundary amplitudes $\delta_T = 0.1$ and $A = 1$ for (a) $Le = 1$ and (b) $Le = 10$.

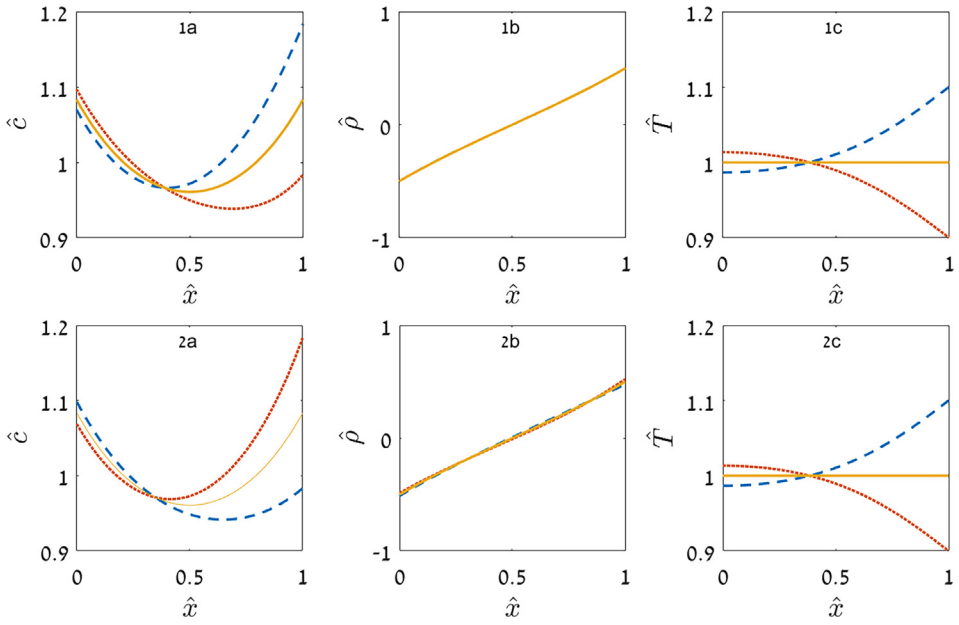

Fig. 8. Combined concentration- and temperature-driven transducer profiles of: (a) dimensionless average salt concentration $\hat{c}$ (b) dimensionless charge density $\hat{\rho}$ (c) dimensionless temperature for (1) minimal phase difference $\theta = 0$ and (2) maximal phase difference $\hat{\omega} = 100$. $\hat{\omega}\hat{t} = 0$ (blue dash), $\hat{\omega}\hat{t} = \pi$ (red dot) and mean (yellow solid). Calculations made for a scaled applied voltage $\zeta = 1$, thick EDL $\epsilon = 1$, $Le = 1$ and scaled boundary amplitudes $\delta_T = 0.1$ and $A = 1$. (For interpretation of the references to colour in this figure legend, the reader is referred to the web version of this article.)

The frequency response is characterized by the same two frequency regimes identified in each previous case. The highest conversion efficiency is attained by maximizing the phase difference between the two oscillations, $(\theta = \pi)$, while the minimal efficiency is reached when the imposed boundary oscillations are in-phase $(\theta = 0)$. This behavior can be understood in terms of the 'interference' between two 'coherent waves'. As mentioned above, the electric current generation mechanism is based upon EDL capacitance variations attained by elongation and shortening of the characteristic length of the EDL, λ_D. Temperature and bulk concentration manifest as competing effects in terms of EDL expansion and contraction, as they have an opposing influence on the Debye length - while a temperature increase results in EDL expansion, a concentration increase will induce EDL contraction. In an analogy to wave propagation, the oscillations of these two properties can be considered as two 'antiphase coherent waves', whose combined 'interference' is destructive. This situation is depicted in the case of $(\theta = 0)$ in Fig. 8. The synchronization of the two oscillations cancel the EDL expansion, thus yield minimal (approaching zero) response efficiency. As a continuation of this analogy, in order to maximize the efficiency, these two 'coherent waves' must form a 'constructive interference'. This situation is achieved when the two properties oscillate with maximal phase difference, as depicted in the case $\theta = \pi$ in Fig. 8.

In most liquid solvents the EDL expansion mechanism is biased towards a temperature driving force since heat diffusion is much faster than ion diffusion. The frequency response of η in this more realistic case, where Le = 10, is shown in Fig. 7b. Here, the maximum conversion efficiency is attained at a larger phase difference. Furthermore, in-phase oscillations do not cancel each other completely.

3.5. Effect of heat generation and electrostatic work

Another parameter connecting the concentration and temperature oscillations, in a destructive manner, is Π. In the last few

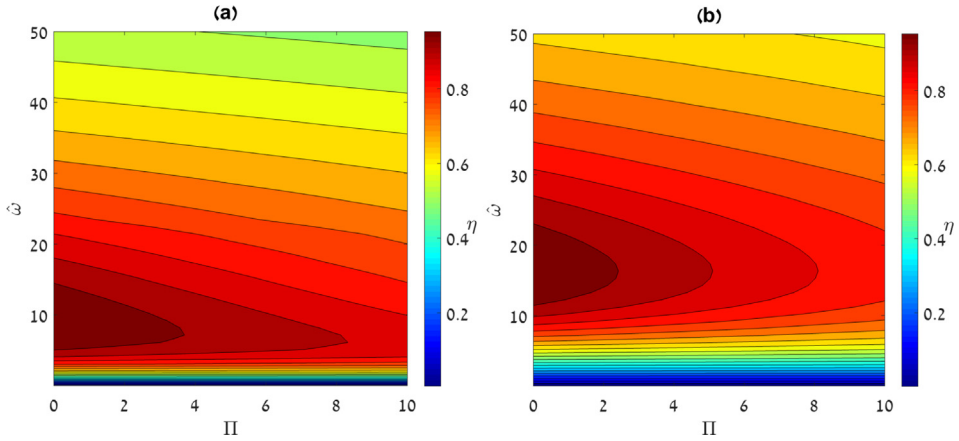

Fig. 9. Current efficiency η of the (a) Concentration-driven transducer and (b) Temperature-driven transducer versus Π and $\hat{\omega}$. Calculations made for a scaled applied voltage $\zeta = 1$, thick EDL $\epsilon = 1$, $Le = 10$ and scaled boundary amplitude $\delta_s = 0.1$ and $\delta_T = 0.1$ respectively.

sections we have illustrated the conversion efficiency for the different cases, in the limit of $\Pi \ll 1$, where the temperature profile is dictated by the temperature oscillations alone, and the generalized Joule heating is negligible. In this section, we wish to investigate the effect of the generalized Joule heating. To quantify the effect of ionic charge transport on temperature, we use the dimensionless quantity $\Pi = 2c_n R/\rho C_p$ appearing in the non-dimensional energy equation, Eq. (6). This quantity may be viewed as representative of the ratio between the system's resistance to changes in concentration, to its resistance to changes in temperature. The frequency response of η, in the concentration and temperature-driven cases, is shown in Fig. 9 for different values of Π.

The most evident conclusion from both Fig. 9 is that lower values of Π yield greater current efficiency, an expected result since these represent lossy mechanisms.

In the limit of $\Pi \ll 1$, the concentration-driven case is characterized by a uniform constant temperature. When Π is no longer negligible, temperature oscillations emerge and their amplitude gets higher as Π increases (Fig. 10b). The effect of Π on current efficiency can be understood through examination of the irreversible heat generation rate in the bulk region that separates the two EDLs (Eq. (6)). As mentioned above, the ionic charge flux must pass a 'resistive' region where the charge flux is mostly dominated by electro-migration of ions and the electric current is governed by Ohm's law. Similar to an electric current flowing through a resistor, this electro-migrative current flowing through the 'resistive' region is characterized by irreversible heat generation. This heating term, $\Pi \frac{\widehat{c}_p}{\widehat{T}_m} \left(\frac{\widehat{\partial \phi_m}}{\widehat{\partial x}} \right)^2$, appearing in Eq. (23), the $O(\delta)$ energy equation, suggests that the temperature oscillations associated with irreversible heat generation are in phase (Fig. 10) with the concentration oscillations. As mentioned in the previous case of combined oscillations, these two properties can be considered as two 'antiphase coherent waves' whose combined 'interference' is destructive, resulting in lower current efficiency.

While higher generalized Joule heating results in more pronounced temperature oscillations in the concentration-driven case, the opposite is true in the temperature-driven case (see Fig. 11). In the limit of $\Pi \ll 1$, the temperature oscillation at the boundary propagates through the domain via conduction. However, in the presence of generalized Joule heating, a significant part of that heat is invested in the electrostatic work required to transfer an ionic charge through the electric field. As Π increases, this energy diversion results in a decreased temperature amplitude, meaning the driving force force EDL expansion is disrupted, and the conversion efficiency declines.

4. Concluding remarks

In this study, we presented a mathematical model describing the physical response and performance of a conceptual electric-double-layer capacitor (EDLC)-based transducer, as it converts periodic concentration and temperature oscillations into an alternating electric current. For simplicity, and in order to make first steps into understanding this interesting device, several assumption have been made that offer interesting paths for future improvement. For example, in this work we restricted ourselves to the case of a fully dissociated, symmetric 1:1 salt and equal, constant diffusion coefficients of the two ionic species. Future work may expand the model into asymmetric electrolytes and consider non-constant transport coefficients. Furthermore, considering a finite ion size with modified PNP equations that account for steric effects [41] and supplementary Stern layer boundary conditions may provide a more accurate picture of the EDLs under confinement. The small amplitude perturbation analysis assumes that the mean problem, which is the time averaged problem per cycle, is only a function of the spatial coordinate. This simplification omits the time-averaged temperature increase due to irreversible heat generation [31]. Furthermore, in this work we considered capacitance variations with constant voltage at the electrodes, generating a zero mean current. Therefore, in this configuration, the EDLC serves only as an energy transducer. Energy harvesting is possible when the EDLC is connected to a resistor [42], in which case the voltage boundary condition at the electrode must consider the resistor's voltage drop, which is dependent on the electric current generated by the EDL modulation.

Through the solution to the model equations, we identified the range of parameters for which the transducer conversion capability is optimal, using a conversion efficiency defined as the ratio of the generated current amplitude to the maximal current amplitude achievable for a given set of parameters. We find that the transducer's optimal performance is governed by two main factors: geometric confinement, namely the minimization of the capacitor thickness, and a resonant frequency dictated by characteristic mass and heat diffusion times. Achieving the former is a requisite for high-frequency operation, but may be challenging to manifest in practice. Furthermore, we concluded that simultaneously occurring temperature and concentration oscillations may have

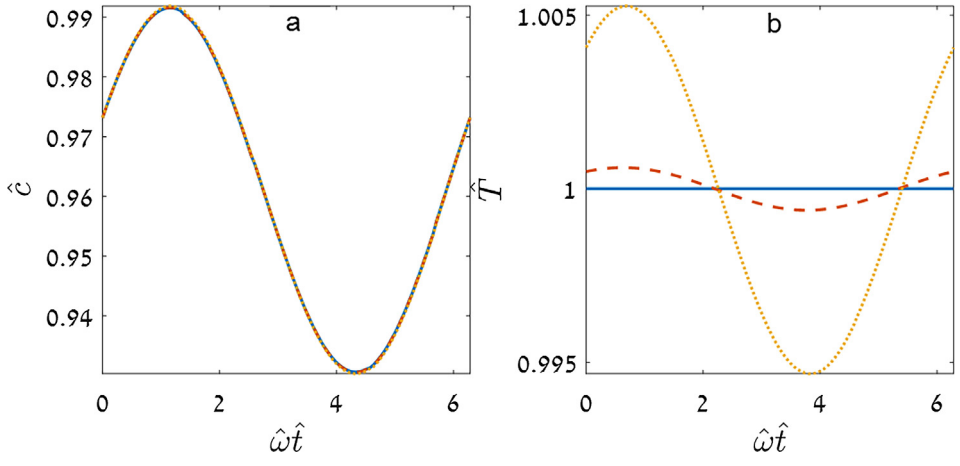

Fig. 10. Concentration-driven transducer time-variation at $\hat{x}_0$, marking the transition point between the EDLs: (a) average salt concentration $\hat{c}$ and (b) dimensionless temperature $\hat{T}$. $\Pi = 0$ (blue solid), $\Pi = 1$ (red dash) and $\Pi = 10$ (yellow dot). Calculations made for a scaled applied voltage $\zeta = 1$, thick EDL $\epsilon = 1$, $Le = 10$ and scaled boundary amplitude $\delta_s = 0.1$. (For interpretation of the references to colour in this figure legend, the reader is referred to the web version of this article.)

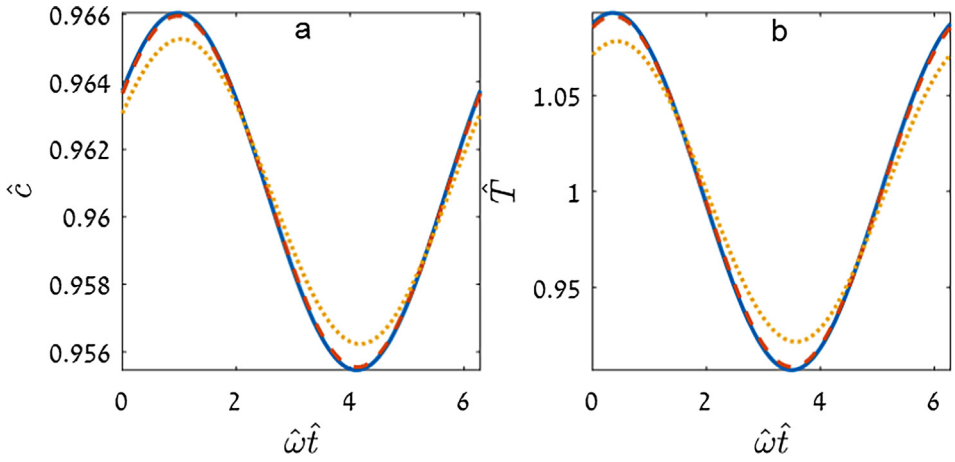

Fig. 11. Temperature-driven transducer time-variation at $\hat{x}_0$, marking the transition point between the EDLs: (a) average salt concentration $\hat{c}$ and (b) dimensionless temperature $\hat{T}$. $\Pi = 0$ (blue solid), $\Pi = 1$ (red dash) and $\Pi = 10$ (yellow dot). Calculations made for a scaled applied voltage $\zeta = 1$, thick EDL $\epsilon = 1$, $Le = 10$ and scaled boundary amplitude $\delta_s = 0.1$. (For interpretation of the references to colour in this figure legend, the reader is referred to the web version of this article.)

competing effects in terms of EDL expansion and contraction. The destructive 'interference' between these two properties can be seen, for example, when both oscillations are in-phase, i.e., $(\theta = 0)$. Furthermore, in the concentration-driven case, temperature oscillations induced by high generalized Joule heating disrupt the driving force for EDL expansion. This also occurs in the temperature-driven case, since a significant part of that heat is invested in parasitic heat sinks rather in temperature variations necessary for enhancing the electro-migrative driving force.

Ultimately, the ability to describe the response of capacitive devices to external stimuli, be it for harvesting naturally occurring fluctuations or engineered systems where such oscillations are controllably produced, represents a promising route to the improved design of efficient devices for real-world applications.

Acknowledgement

I.A. acknowledges the financial support given by the Nancy and Stephen Grand Technion Energy Program (GTEP).

References

[1] S. Meninger, J.O. Mur-Miranda, R. Amirtharajah, A. Chandrakasan, J.H. Lang, Vibration-to-electric energy conversion, IEEE Trans. Very Large Scale Integr. Syst. 9 (1) (2001) 64–76.
[2] Y. Naruse, N. Matsubara, K. Mabuchi, M. Izumi, S. Suzuki, Electrostatic micro power generation from low-frequency vibration such as human motion, J. Micromechanics Microengineering 19 (9) (2009).
[3] S. Boisseau, G. Despesse, B.A. Seddik, Electrostatic conversion for vibration energy harvesting, Small-Scale Energy Harvest. (2012) 1–39. Available from: arXiv:1210.519.
[4] F. Wang, O. Hansen, Electrostatic energy harvesting device with out-of-the-plane gap closing scheme, Sens. Actuators, A Phys. 211 (2014) 131–137.
[5] Y. Suzuki, Electrostatic/Electret-Based Harvesters, Micro Energy Harvest, Vol. 2, Wiley-VCH Verlag, GmbH & Co. KGaA, 2015, pp. 149–174. Available from: arXiv:9809069v1.
[6] P. Sharma, T.S. Bhatti, A review on electrochemical double-layer capacitors, Energy Convers. Manag. 51 (12) (2010) 2901–2912.
[7] R.F. Probstein, Physicochemical Hydrodynamics, Second ed., Wiley, 1994.
[8] E. Gongadze, S. Petersen, U. Beck, U.V. Rienen, Classical models of the interface between an electrode and an electrolyte, In: Proc. COMSOL Conf. Milan. (2009).
[9] S. Kondrat, A. Kornyshev, R. Qiao, Two tributaries of the electrical double layer, J. Phys. Condens. Matter 28 (46) (2016) 460301.
[10] J.K. Moon, J. Jeong, D. Lee, H.K. Pak, Electrical power generation by mechanically modulating electrical double layers, Nat. Commun. 4 (2013) 1487.
[11] S. Yamada, H. Mitsuya, H. Fujita, Vibrational energy harvester based on electrical double layer of ionic liquid, J. Phys. Conf. Ser. 557 (2014) 012013.
[12] M. Janssen, B. Werkhoven, R. van Roij, Harvesting vibrational energy with liquid-bridged electrodes: thermodynamics in mechanically and electrically driven RC-circuits, RSC Adv. (2016) 20485–20491. Availble from: arXiv:1603.0431.
[13] D.H. Huynh, T.C. Nguyen, P.D. Nguyen, C.D. Abeyrathne, M.S. Hossain, R. Evans, E. Skafidas, Environmentally friendly power generator based on moving liquid dielectric and double layer effect, Sci. Rep. 6 (January) (2016) 26708.
[14] Y. Yang, J. Park, S.-H. Kwon, Y.S. Kim, Fluidic active transducer for electricity generation, Sci. Rep. 5 (2015) 15695.
[15] Y. Gao, J. Song, S. Li, C. Elowsky, Y. Zhou, S. Ducharme, Y.M. Chen, Q. Zhou, L. Tan, Hydrogel microphones for stealthy underwater listening, Nat. Commun. 7 (2016) 1–10.
[16] E. Virga, W.M. De Vos, P.M. Biesheuvel, Theory of gel expansion to generate electrical energy, Epl. 120 (4) (2017).
[17] D. Brogioli, Extracting renewable energy from a salinity difference using a capacitor, Phys. Rev. Lett. 103 (5) (2009) 31–34.
[18] D. Brogioli, R. Ziano, R.a. Rica, D. Salerno, O. Kozynchenko, H.V.M. Hamelers, F. Mantegazza, Exploiting the spontaneous potential of the electrodes used in the capacitive mixing technique for the extraction of energy from salinity difference, Energy Environ. Sci. 5 (2012) 9870–9880.
[19] R.A. Rica, R. Ziano, D. Salerno, F. Mantegazza, M.Z. Bazant, D. Brogioli, Electro-diffusion of ions in porous electrodes for capacitive extraction of renewable energy from salinity differences, Electrochim. Acta 92 (2013) 304–314.
[20] B. Shapira, E. Avraham, D. Aurbach, The feasibility of energy extraction from acidic wastewater by capacitive mixing with a molecular-sieving carbon electrode, ChemSusChem 9 (24) (2016) 3426–3433.
[21] H.V.M. Hamelers, O. Schaetzle, J.M. Paz-García, P.M. Biesheuvel, C.J.N. Buisman, Harvesting energy from CO_2 emissions, Environ. Sci. Technol. Lett. 1 (1) (2014) 31–35.
[22] J.M. Paz-Garcia, J.E. Dykstra, P.M. Biesheuvel, H.V.M. Hamelers, Energy from CO_2 using capacitive electrodes - a model for energy extraction cycles, J. Colloid Interface Sci. 442 (2015) 103–109.
[23] A. Härtel, M. Janssen, D. Weingarth, V. Presser, R. van Roij, Heat-to-current conversion of low-grade heat from a thermocapacitive cycle by supercapacitors, Energy Environ. Sci. (2015) 2396–2401.
[24] C. Guthy, C.W. Van Neste, S. Mitra, S. Bhattacharjee, T. Thundat, Parametric energy conversion of thermoacoustic vibrations, Appl. Phys. Lett. 100 (20) (2012) 1–5.
[25] D. Zabek, J. Taylor, V. Ayel, Y. Bertin, C. Romestant, C.R. Bowen, A novel pyroelectric generator utilising naturally driven temperature fluctuations from oscillating heat pipes for waste heat recovery and thermal energy harvesting, J. Appl. Phys. 120 (2) (2015).
[26] G.W. Swift, Thermoacoustic engines, J. Acoustical Soc. Am. 84 (4) (1988) 1145.
[27] M.Z. Bazant, K. Thornton, A. Ajdari, Diffuse-charge dynamics in electrochemical systems, Soft Matt. Phys. 70 (2 1) (2004) 1–24. Available from: arXiv:040111.
[28] M. Van Soestbergen, P.M. Biesheuvel, M.Z. Bazant, Diffuse-charge effects on the transient response of electrochemical cells, Phys. Rev. E - Stat. Nonlinear, Soft Matt. Phys. 81 (2) (2010) 1–13.
[29] L. Højgaard Olesen, M.Z. Bazant, H. Bruus, Strongly nonlinear dynamics of electrolytes in large ac voltages, Phys. Rev. E 82 (1) (2010) 1–29. Available from: arXiv:0908.350.
[30] M. Schmuck, M. Bazant, Homogenization of the Poisson-Nernst-Planck equations for ion transport in charged porous media, SIAM J. Appl. Math. 75 (3) (2015) 1369–1401.
[31] A. D'Entremont, L. Pilon, First-principles thermal modeling of electric double layer capacitors under constant-current cycling, J. Power Sources 246 (2014) 887–898.
[32] A. D'Entremont, L. Pilon, Scaling laws for heat generation and temperature oscillations in EDLCs under galvanostatic cycling, Int. J. Heat Mass Transf. 75 (2014) 637–649.
[33] A.L. D'Entremont, L. Pilon, Thermal effects of asymmetric electrolytes in electric double layer capacitors, J. Power Sources 273 (2015) 196–209.

[34] S.R. de Groot, Thermodynamics of Irreversible Processes, North-Holland, Amsterdam, 1951.
[35] W.B. Gu, C.Y. Wang, Thermal-electrochemical modeling of battery systems, J. Electrochem. Soc. 147 (8) (2000) 2910.
[36] P.M. Biesheuvel, D. Brogioli, H.V.M. Hamelers, Negative Joule Heating in Ion-Exchange Membranes i (2014) 1–6. arXiv:1402.1448.
[37] R.F. Stout, A.S. Khair, Moderately nonlinear diffuse-charge dynamics under an ac voltage, Soft Matt. Phys. 92 (3) (2015) 1–12.
[38] W. Qu, D. Li, A model for overlapped EDL fields, J. Colloid Interface Sci. 224 (2) (2000) 397–407.
[39] S.E. Feicht, A.E. Frankel, A.S. Khair, Discharging dynamics in an electrolytic cell, Phys. Rev. E - Stat. Nonlinear, Soft Matt. Phys. 94 (1) (2016) 1–13.
[40] M. Janssen, M. Bier, Transient dynamics of electric double layer capacitors: Exact expressions within the Debye-Falkenhagen approximation, Phys. Rev. E 97 (5) (2018) 052616.
[41] M.S. Kilic, M.Z. Bazant, A. Ajdari, Steric effects in the dynamics of electrolytes at large applied voltages. II. Modified Poisson-Nernst-Planck equations, Phys. Rev. E 75 (2) (2007) 1–11. Available from: arXiv:061123.
[42] T. Krupenkin, J.A. Taylor, Reverse electrowetting as a new approach to high-power energy harvesting, Nat. Commun. 2 (448) (2011) 1–7.